Thermodynamics behind Carbon Nanotube Growth *via* Endothermic Catalytic Decomposition Reaction

Avetik R. Harutyunyan,* Oleg A. Kuznetsov, Christopher J. Brooks, Elena Mora, and Gugang Chen

Honda Research Institute USA Inc., 1381 Kinnear Road, Columbus, Ohio 43212

ABSTRACT Carbon filaments can be grown using hydrocarbons with either exothermic or endothermic catalytic decomposition enthalpies. By *in situ* monitoring the evolution of the reaction enthalpy during nanotube synthesis *via* methane gas, we found that although the decomposition reaction of methane is endothermic an exothermic process is superimposed which accompanies the nanotube growth. Analysis shows that the main contributor in this liberated heat is the radiative heat transfer from the surroundings, along with dehydrogenation reaction of *in situ* formed secondary hydrocarbons on the catalyst surface and the carbon hydrogenation/oxidation processes. This finding implies that nanotube growth process enthalpy is exothermic, and particularly, it extends the commonly accepted temperature gradient driven growth mechanism to the growth *via* hydrocarbons with endothermic decomposition enthalpy.

KEYWORDS: carbon fibers · carbon nanotubes · growth mechanism · thermodynamics · chemical vapor deposition

Although considerable effort and progress has been made in carbon filaments synthesis, the growth mechanism is not fully understood yet and remains a hotly debated area.[1−8] The concept of carbon filament growth through carbon diffusion in the catalyst is based upon the agreement between the activation enthalpy of carbon diffusion and the enthalpy for the growth of filament.[1,9] There are two main hypotheses about the origin of the driving force for diffusion.[1,10] The commonly accepted mechanism,[1] postulated in 1972 by Baker, implies an exothermic decomposition of the hydrocarbon on an exposed facet of the metallic catalyst particle and the endothermic reaction of carbon precipitation on the opposite face of the particle. These reactions sustain a temperature gradient across the particle, which becomes the driving force for filament growth. However, this mechanism is valid only for hydrocarbons with exothermic decomposition and contradicts successful experimental results of filament growth by hydrocarbons with endothermic dehydrogenation reaction. To explain this inconsistency, the presence of admixtures or secondary hydrocarbons[2,11] with exothermic decomposition (C_2H_4, C_2H_2, *etc.*) or compensation of the endothermic decomposition by heat radiation from the environment[12] have been suggested. Some of these suggestions were disproved,[13] while others are unfeasible due to the nature of thermodynamic studies on the level of individual nanoparticles.[14] It was recently reported that the deposition of various forms of carbon occurs not directly from used feedstock molecules but from intermediate reaction products.[15] Moreover, it has been reported that the presence of active carbon species, such as ethylene and acetylene, is essential for growth of SWCNTs *via* methane gas.[16] Another mechanism driven by a temperature gradient, but without resorting to exothermicity of hydrocarbon decomposition, was described in 1989, which suggests that the temperature gradient across the particle is maintained by the endothermic graphite precipitation at the graphite/metal interface and the exothermic carbon dissolution at the gas/metal interface.[12] However, this scenario cannot explain the onset of the precipitation. An alternative concept, the concentration gradient driven growth model,[10] is deduced from the idea of supersaturation of carbon in the catalyst at the gas/metal interface when the activity of carbon in the gas phase exceeds unity. Carbon filament growth involves formation of carbon atoms on the catalyst surface, dissolution in the metal, and precipitation out at a dislocation on an opposing side of the particle. However, the metals in which supersaturation does not occur also provide filaments.[10] Hence, careful energetic and thermodynamic analysis of the carbon precursor interaction with the

*Address correspondence to aharutyunyan@honda-ri.com.

Received for review September 3, 2008 and accepted January 19, 2009.

Published online January 29, 2009.
10.1021/nn8005569 CCC: $40.75

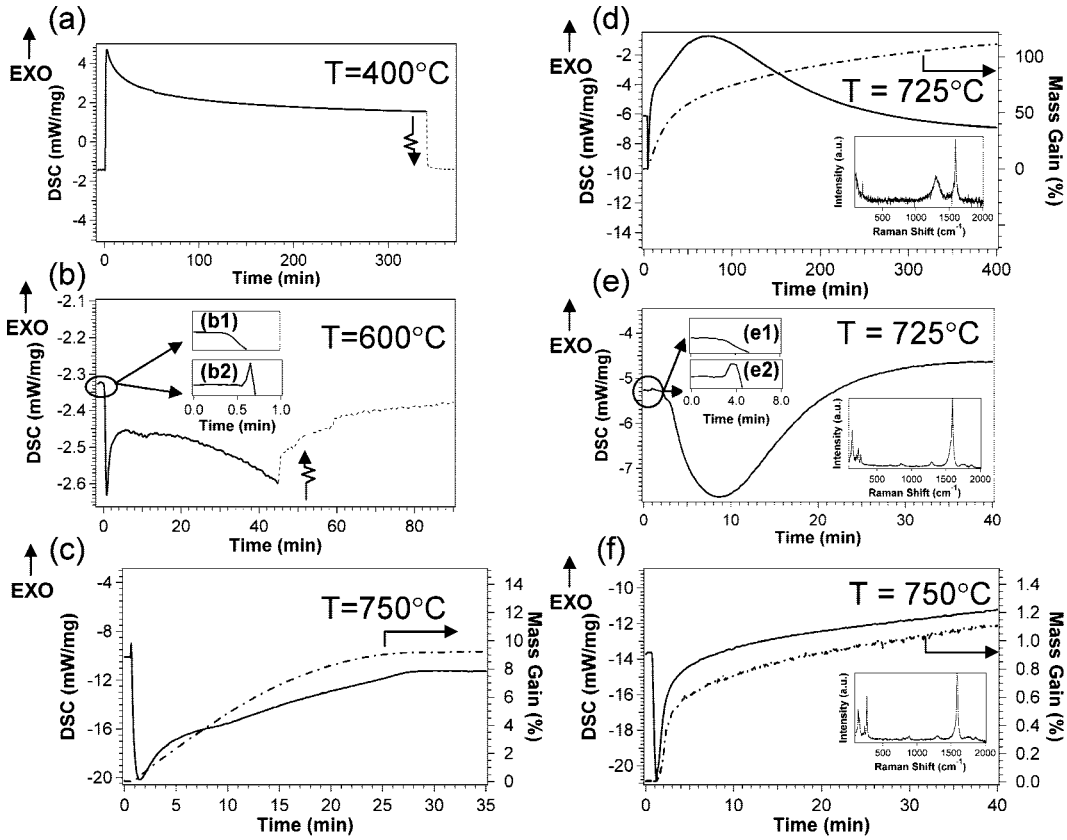

Figure 1. Heat flow profiles for Pd/Al_2O_3 (left panels) and $(Fe/Mo)/Al_2O_3$ (right panels) catalysts during SWCNTs growth when C_2H_4 (panels a and d) and CH_4 (panels b, c, e, and f) gases are used as carbon source. The arrows in (a) and (b) show the "relaxation" of the signal (dash line) toward the baseline upon switching off the carbon source. Insets in (b) and (e) show the initial exothermic small signals in case of deeply oxidized catalyst (b2 and e2) compared with preliminarily reduced under H_2 catalyst (b1 and e1). The lower insets in panels d−f show the Raman spectra for the carbon deposits collected after the experiments.

catalyst and the following carbon nanotube growth process is critical for understanding the growth mechanism. To this end, a new opportunity arises when the hydrocarbon decomposition reaction enthalpy during SWCNT synthesis is followed *in situ* in a differential scanning calorimeter (DSC), with simultaneous evaluation of carbon uptake (by thermal gravimetrical analysis, TGA) and exhaust gas composition (by mass spectrometry, MS, and gas chromatography, GC).

RESULTS AND DISCUSSION

Figure 1a shows the exothermic heat flow profile ($\Delta[dQ/dt] > 0$ for particular setup; Q is the heat of reaction and Δ denotes the heat flow difference between sample and reference) for ethylene decomposition reaction at 400 °C on Pd catalyst, used here as a standard heat profile. This heat flow profile fits the decomposition reaction: $C_2H_4 \rightarrow 2C + 2H_2$. On the other hand, methane decomposition reaction at $T = 600$ °C on the same Pd catalyst is moderately endothermic ($\Delta[dQ/dt] < 0$, Figure 1b), and the obtained calorimetric signal can be attributed to the following reaction:[17] $CH_4 \rightarrow C + 2H_2$. TG and Raman measurements show that higher temperature promotes the carbon formation on the catalyst surface, affecting the heat flow kinetics (Figure 1c). Similarly, Figure 1d,e shows the heat flow profiles for exothermic and endothermic decomposition reactions of C_2H_4 and CH_4 hydrocarbons over the Fe/Mo catalyst at 725 °C, respectively. For both hydrocarbons, Raman measurements confirm the growth of SWCNTs (lower insets in Figure 1d,e).

In order to analyze the reaction enthalpy and its origin, the shape of the heat profile and the position of the baseline are very important. For the decomposition of ethylene at $T = 400$ °C (Figure 1a, no carbon formation), the heat flow was sustained while ethylene was provided, and after termination of the hydrocarbon flow, the signal moved back to the initial baseline (Figure 1a, dashed line). However, in the case of methane decomposition at $T = 600$ °C, the signal does not reach completely the initial baseline upon termination of the hydrocarbon flow (Figure 1b, dashed line), due to some carbon formation on the sample. The formation of more carbon on the catalyst surface at even higher temperatures slows down and eventually terminates the decomposition of the hydrocarbon (Figure 1c,e,f), observing a decrease and cease of the heat flow. More importantly, and as will be shown later, the position of the final baseline is dramatically different from the initial one. Indeed, the distinction of our experiments is

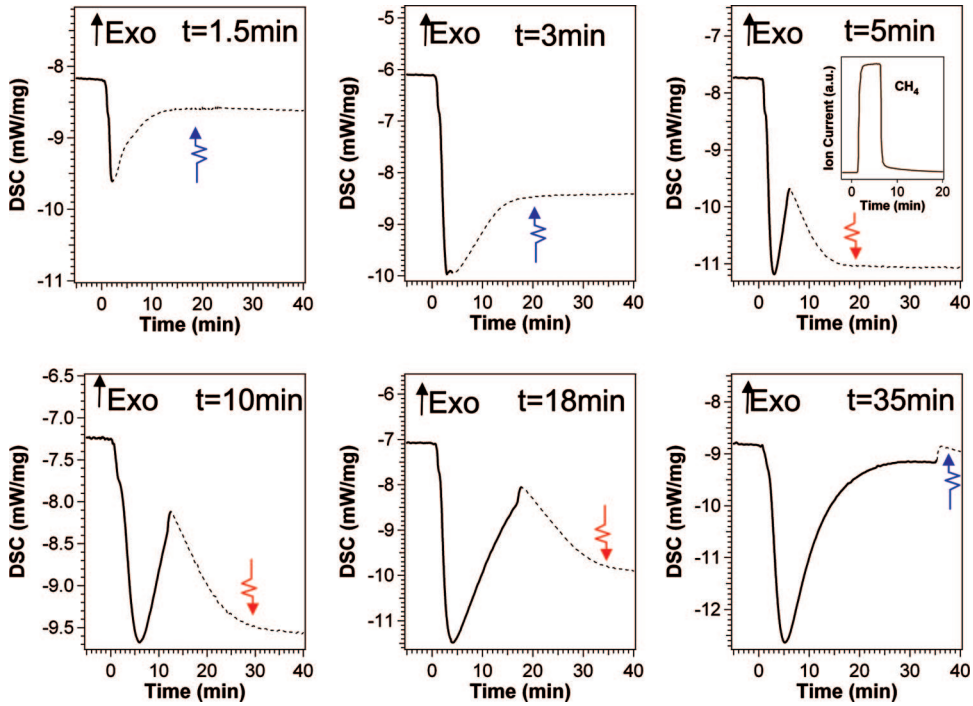

Figure 2. Evolution of the heat flow profiles upon switching off methane gas at different time periods at $T = 725$ °C. Blue and red arrows indicate the endothermic and exothermic character of the "relaxation" toward the baseline, respectively. The inset shows the CH_4 gas level according to MS.

that the heat flow is described according to the following expression:

$$dQ/dt = d(C \cdot m \cdot T)/dt \quad (1)$$

where Q is the heat flow, C is the specific heat, m is the mass, and T is the given sample temperature that can vary due to the reactions. For typical DSC measurements $C \neq C(t)$ and $m \neq m(t)$, and dT/dt is the temperature scan rate of the reactor. However, during nanotube growth, both the specific heat (C) and the thermoconductivity (λ) undergo dramatic changes if we take into account the values[18] $C_{cat} = 970$ J/kg · K, $C_{NT} = 1542$ J/kg · K, $\lambda_{cat} = 0.032$ W/m · K (for bulk density $\rho \sim 2.2$ g/cm^3) and $\lambda_{NT} \sim 3000$ W/m · K. In addition, there is a large mass uptake (up to 30 wt %), a change in radiation heat flux $\sim\sigma T^4$ (σ is the Stefan's constant), and significant morphology changes as the Brunauer−Emmett−Teller (BET) surface area decreases from 342 to 43 m^2/g. These alterations significantly contribute to the sample/crucible thermal coupling, and thereby, one would expect that the ability to measure the absolute heat flow would change throughout the experiment, leading to changing signal and a moving baseline. The latest is particularly important to analyze the reaction enthalpy, as the origin of the signal (exo/endo) is defined according to the position of the signal relative to the baseline (according to Figure 1a: $\Delta[dQ/dt] > 0$ describes the exothermic nature of heat flow, while according to Figure 1b, $\Delta[dQ/dt] < 0$ corresponds to endothermic reactions).

In order to follow the evolution of the baseline throughout the synthesis and, therefore, to be able to study in detail the evolution of the reaction enthalpy and its origin during SWCNT synthesis *via* methane decomposition, a series of samples were prepared at 725 °C with different synthesis duration (Figure 2): $t = 1.5$ and 3 min (the period when signal increases), $t = 5$, 10, 11, 18, and 21 min (the period when signal decreases), and $t = 35$ and 41 min (very slight evolution of heat flow). At the given time, we terminated the CH_4 gas flow, leaving all other parameters unchanged (the complete heat flow profile during SWCNT growth at 725 °C is shown in Figure 1e). Termination of the hydrocarbon supply results in the discontinuation of the heat flow dQ/dt, and one should expect the return of the signal to the initial baseline. For synthesis durations of $t < 3$ min, the ongoing endothermic reaction ($\Delta[dQ/dt] < 0$) stopped with the flow of methane, and the signal returned toward the baseline (Figure 2), which, however, is already different from the initial baseline. Further, the baselines of the samples prepared for $t >$ 3 min moved significantly relative to the initial baseline, in agreement with above-described sensitivity of the baseline on the state of the sample.

Importantly, these series of experiments allow us to reveal the actual baseline during the synthesis of SWCNTs with methane at 725 °C. The curve is shown in Figure 3a (red dashed curve), where $\Delta_{Baseline}$ is defined as the difference between the initial baseline and its final value (the value detected after ~40−60 min of stabilization of the system upon termination of the meth-

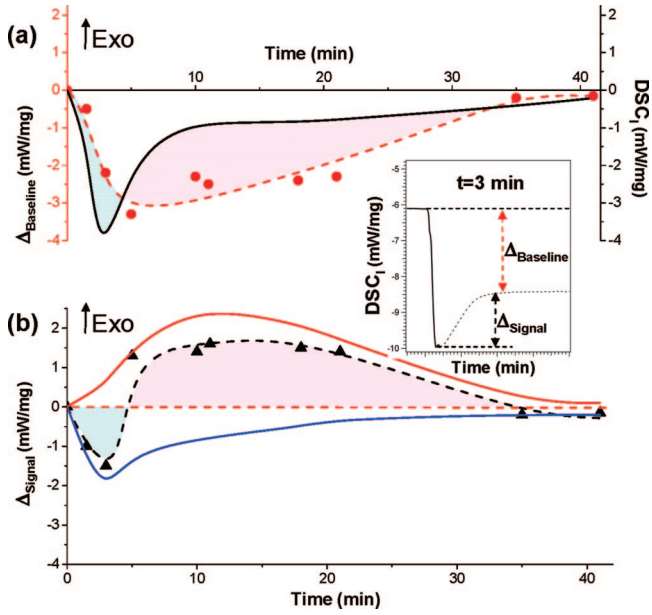

Figure 3. Evolution of (a) the actual baseline ($\Delta_{Baseline}$, red dashed curve) and the heat flow profile (black curve) and (b) the heat flow profile relative to the baseline (Δ_{Signal}, black dashed curve), during the synthesis of SWCNTs over (Fe/Mo)/Al_2O_3 catalyst with methane at 725 °C. In panel b, the solid blue and red lines represent possible endothermic and exothermic profiles whose combination could result in the actual heat flow profile (dashed black line). The inset shows how the values of $\Delta_{Baseline}$ (difference between the initial baseline and its final value detected after ~40−60 min of stabilization of the system upon termination of the methane flow) and Δ_{Signal} (difference between the heat flow values for the signal at the moment of termination of the methane flow and the corresponding actual baseline) are obtained. The shadow areas correspond to $\Delta[dQ/dt] < 0$ (blue color, endothermic) and $\Delta[dQ/dt] > 0$ (red color, exothermic).

ane flow); see inset in Figure 3. It is remarkable that for synthesis durations $t > 3$ min the actual signal (black curve) crosses the baseline (red dashed curve), which means that the heat flow changes sign from $\Delta[dQ/dt] < 0 \rightarrow \Delta[dQ/dt] > 0$ and corresponds to an endo → exo transition. Physically it implies that the heat flow to the sample became less than the heat flow to the reference pan in the DSC apparatus. This transition is confirmed by following the "relaxation" of the signal (arrows in Figure 2) toward the baseline ($d|\Delta[dQ/dt]|/dt < 0$). In fact, upon termination of the heat flow, the signals for the samples prepared for $t < 3$ min and for $t > 5$ min reach the baseline from opposite sides, which is another distinctive characteristic of the different nature of the signals. Further increase of the reaction period $t \geq 35$ min again results in the behavior typical for termination of an endothermic reaction $\Delta[dQ/dt] < 0$ relative to the corresponding baseline (Figure 2). For clarity, the evolution of the heat flow profile during nanotube growth is plotted relative to the *actual baseline* in Figure 3b. Here, the values of the enthalpies (Δ_{Signal}, black dashed curve) correspond to the difference between the heat flow values for the signal at the moment of termination of the methane flow and the corresponding *actual baseline* (see inset in Figure 3), taking into account also the position of the signal with regards to the baseline ($\Delta_{Signal} - \Delta_{Baseline} < 0$ and $\Delta_{Signal} - \Delta_{Baseline} > 0$). The graph (Figure 3b, black dashed curve) shows that during nanotube synthesis the overall reaction enthalpy changes from endothermic to exothermic in the period between 5 and 30 min, which we attribute to exothermic (red line) processes that accompany the endothermic methane decomposition (blue line).

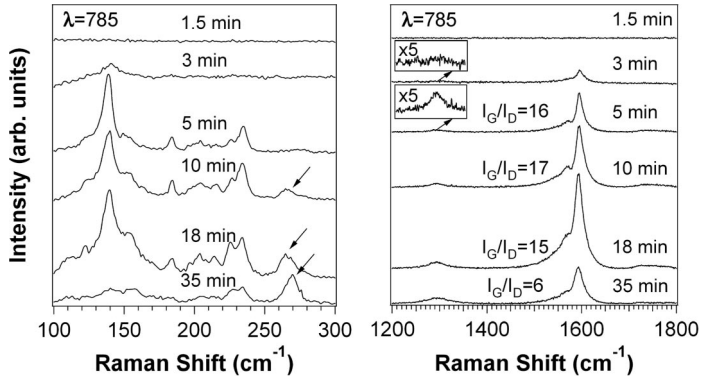

Figure 4. Evolution of Raman breathing modes (RBM, left panel) and tangential modes (right panel) for the samples obtained at different period of SWCNT growth at $T = 725$ °C with methane. The arrows indicate the RBM for smaller diameter tubes.

To validate the period favorable for the growth of SWCNTs and its relationship with the type of reaction enthalpy, we performed Raman studies of the samples synthesized at the different time periods. The spectra (Figure 4) show no SWCNT formation during the initial endothermic reaction period $t < 3$ min (some trace is observed for $t = 3$ min), while increasing the reaction duration ($t \geq 5$ min) leads to the appearance of RBM and G-band modes, the evidence of SWCNTs. Importantly, the period for detection of SWCNT growth coincides with the period of significant exothermic contribution superimposed over the methane endothermic signal. Moreover, analysis of the grown SWCNT quality (the ratio of G- and D-band intensities, I_G/I_D) revealed that the decrease of exothermic contribution results in a decline of the tubes quality ($I_G/I_D \sim 16$ for reaction times 5−18 min, while $I_G/I_D \sim 6$ for $t \geq 35$ min), even though there is still detectable carbon uptake observed according to TG results. This suggests that the carbon formed after 35 min is mainly sp^2 carbon disordered structures. Interestingly, in the growth period when significant heat is liberated ($t \geq 10$ min), we observed formation of small diameter tubes with $d \sim 0.9$ nm (using $\omega = 223.75/d + 14$, where ω is the Raman frequency). One possible explanation for this observation is the increased formation energy of the tubes with decreasing diameter due to the curvature energy.[19,20]

Finally, we tried to reveal the origin of the exothermic process occurring during methane decomposition. For this purpose, we carried out an *in situ* MS evaluation of the product gas species along with the calorimetric measurements during nanotube synthesis. Various active hydrocarbon species with exothermic catalytic de-

composition reactions (*e.g.*, C_2H_2, C_2H_4) were detected in the outlet gas of the reactor at the very beginning of the synthesis $t < 5$ min (Figure 5a), which is in agreement with previous reports.[15,16] The analysis of the initial CH_4 gas composition without catalyst shows no detectable presence of these species. We assume that these are the products of the coupling of CH_4 fragments on the catalyst surface:

$$2CH_4 \xrightarrow{\Delta H = 202.3\text{kJ/mol}}$$

$$C_2H_4 + 2H_2 \xrightarrow{\Delta H = -52.5\text{kJ/mol}} 2C(\text{solid}) + 4H_2 \quad (2)$$

$$2CH_4 \xrightarrow{\Delta H = 376.5\text{kJ/mol}}$$

$$C_2H_2 + 3H_2 \xrightarrow{\Delta H = -226.7\text{kJ/mol}} 2C(\text{solid}) + 4H_2 \quad (3)$$

In order to distinguish in the MS between C_2H_4 and CO species (same atomic mass 28), we used isotopically labeled ^{13}C methane to grow the nanotubes. The resulting product shows the presence of both species. Hence, endothermic decomposition of the methane on the catalyst surface results in the formation of secondary hydrocarbons, whose further catalytic decomposition is accompanied with heat release. Yet, we cannot exclude formation of other intermediate species (*e.g.*, radicals) on the catalyst surface that may contribute to the overall enthalpy of the process. Formation of secondary hydrocarbons is also independently confirmed by GC analysis (Figure 5b). This result is in agreement with ref 16, where authors confirmed the conversion of CH_4 into C_2H_2 and C_2H_4 by *in situ* FT-IR during SWCNT growth *via* CH_4 and believed that these molecules produce active carbon precursors for nanotube growth. The fact of the formation of species with exothermic dissociation reactions was used in ref 21 to understand the mechanism of nanotube forest growth termination. Taking into account the ratios between the enthalpies of dehydrogenation reactions of secondary hydrocarbons (2) and methane (3), as well as the conversion ratios (Figure 5), it is obvious that the exothermic decomposition of secondary hydrocarbons cannot provide enough energy for altering the reaction enthalpy from endothermic to exothermic.

Remarkably, upon the termination of the methane flow, but in the presence of hydrogen gas flow (20 sccm) at synthesis temperature $T = 725$ °C, the *in situ* TG analysis shows a noticeable (10−30%) initial decrease of the carbon uptake weight before stabilization. This experimental fact is attributed to the reverse reaction of CH_4 decomposition, carbon etching,[22] that is the reaction of attached carbon on the catalyst surface with the hydrogen to create different species of hydrocarbon: C(solid) + $H_2 \rightarrow C_nH_m$(gas), $\Delta H < 0$. In general, during nanotube growth, both types of reactions are present, yet the optimization of the condition makes the equilibrium of methane decomposition shift to the direction favorable for hydrogen and nanotube production. These reverse reactions are another source of exothermic enthalpy, but still this cannot change the overall reaction enthalpy sign. As one can see in Figure 5, MS and GC measurements show also formation of CO and CO_2 during nanotube growth. We exclude the detectable presence of the gas phase oxygen in the reactor because the experiments under analogous conditions but without sample did not reveal these species. Since the catalyst contains Fe, the presence of residual oxygen even after thorough prereduction is very likely.[23,24] This can lead to a methane decomposition path through intermediate reactions analogous to $CH_4 + Fe_2O_3 \rightarrow Fe + C(\text{solid}) + CO_2 + H_2O$ with enthalpies $\Delta H < 0$ (*e.g.*, $C + O_2 \rightarrow CO_2$, $\Delta H = -394$ kJ/mol at $T = 700$ °C) or its derivatives. However, systematic studies of the evolution of CH_4 decomposition reaction enthalpy on thoroughly reduced (72 h under H_2 flowing at 500 °C) or deeply oxidized (72 h under pure O_2 flowing at 500 °C) samples show that deep oxidation of catalyst results in a small initial exothermic peak followed by a strong endothermic signal (Figure 1e insets). We independently confirmed this result by using Pd catalysts that had undergone the same treatments (Figure 1b insets). It seems that the enthalpy of these reactions in the initial stage is suppressed by the relative stronger endothermic reaction, while the absorption of more carbon on the catalyst surface promotes the formation of CO and CO_2 and thereby the exothermic heat flow contribution. However, these reactions alone also cannot change the overall enthalpy sign. Indeed, considering an average carbon uptake yield ~20 wt % (for Fe/Mo/Al_2O_3 = 1:0.21:16 catalyst) and assuming that all carbon is formed through the ideal reaction $CH_4 \rightarrow C + 2H_2$ with $\Delta H = 75$ kJ/mol, we found that for compensation of this endothermic heat by the exothermic reac-

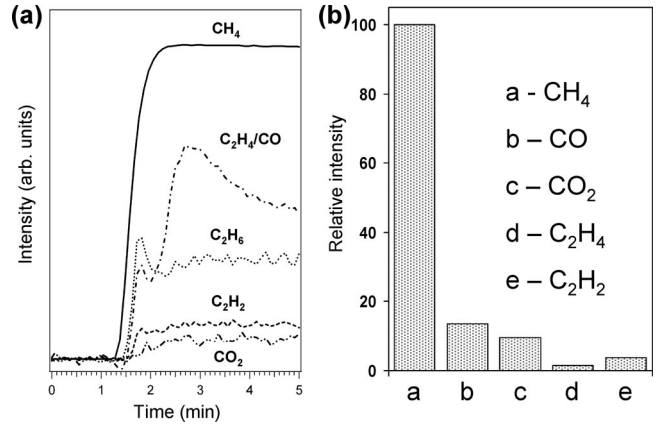

Figure 5. Exhaust gas composition analysis results by MS (a) and GC (b) obtained for the growth of SWCNTs *via* methane gas decomposition at $T = 725$ °C for the period of $t = 5$ min.

tion $C + O_2 \rightarrow CO_2$ with $\Delta H = -394$ kJ/mol it requires 1 order of magnitude more oxygen concentration than Fe_2O_3 or Fe_3O_4 provides.

In the meantime, this analysis shows that the presence of oxidizing environment (O_2, H_2O) during nanotube growth can make this path of enthalpy alteration dominant. For instance, alteration of enthalpy of heat flow during nanotube growth can be another role of the water in the water-assisted growth of SWCNTs.[25]

Finally, another source of heat is the radiative heat transferred from the surroundings to the sample during nanotube growth described by

$$\Theta_R = e\sigma A(T^4_{\text{reactor}} - T^4_{\text{particle}}) \quad (4)$$

where Θ_R is the heat flux, e is the emissivity, and A is the surface area of the object. This effect can be significant if taking into account that during nanotube growth the sample changes its emissivity dramatically. Indeed, according to our estimation based on the calorimetric curve (Figure 1e), the sample temperature can vary up to ~1−3 °C (assuming $e = 1$) during the period of methane decomposition. This corresponds to a heat transfer from the environment of ~3 mW/mg that can compensate the endothermic decomposition. Thus, the total heat provided to the catalyst during actual nanotube growth *via* methane decomposition can be described by the expression

$$d\Theta/dt = \sum_i \Delta H_i \cdot [dN_i/dt] + \sum_j \Delta H_j \cdot [dN_j/dt] + d\Theta_R/dt \quad (5)$$

where ΔH_i is the enthalpy of the reaction, dN_i/dt and the dN_j/dt are the hydrocarbon decomposition and carbon hydrogenation/oxidation rates, correspondingly, at given temperature, i,j denote the active endothermic ($\Delta H > 0$) and exothermic ($\Delta H < 0$) species, and the sum is taken over all active species, and Θ_R is the radiative heat flux. Hence, even though the decomposition reaction of methane gas is endothermic, in actual synthesis conditions, there is a significant exothermic heat that superimposes it, which converts the overall reaction into exothermic and accompanies the nanotube growth. Particularly, under our experimental conditions, the dominant contribution in the reaction heat is the heat radiation from the surroundings. Analysis and models indicate that one needs to consider the following relatively independent stages for growth of a carbon nanotube, each one of them requiring thermal activation: (a) decomposition of carbon feedstock yielding carbon atoms, (b) diffusion of these atoms in or on the catalyst particle, and (c) incorporation of the carbon atoms into the tube structure.[24,26−30] We think that one possible scenario for utilization of the observed released energy is overcoming the carbon atoms diffusion barrier (from ~0.4 up to 1.8 eV) on or into the catalyst particle.

The implication of the findings presented here is that any modification of nanotube synthesis conditions (*e.g.*, adding H_2O, O_2, H_2, CO, ..., gases) or catalyst composition (*e.g.*, oxide forms, adding Mo, Al, ...) should be considered also from the point of view of the thermodynamics, particularly their contribution in the overall reaction enthalpy during interaction with carbon source or gaseous environment at a given temperature. This is particularly crucial for nanotube growth *via* hydrocarbons with endothermic catalytic dehydrogenation reactions. It is worth noting that our result rules out the basic argument of Baker's model opponents described above, although it is still necessary to study the viability of the generation of a significant temperature gradient across such small catalyst particles with high thermal conductivity.

CONCLUSION

The enthalpy of SWCNT synthesis process *via* methane gas was evaluated *in situ* by calorimetry measurements. The study establishes that the actual growth of SWCNTs is accompanied by exothermic reaction, even when using a hydrocarbon with endothermic catalytic decomposition such as methane. This exothermic enthalpy is mainly attributed to the heat flow due to the radiative heat transfer from the surroundings along with catalytic dehydrogenation of *in situ* formed secondary hydrocarbons and carbon hydrogenation/oxidation processes.

EXPERIMENTAL SECTION

Catalyst Preparation and Characterization. Alumina aerogel supported bimetallic Fe/Mo catalyst (molar ratio $Fe/Mo/Al_2O_3$ of 1:0.2:16) was prepared by sol−gel method followed by supercritical drying; 5.28 g of aluminum *sec*-butoxide (97%, Alfa Aesar) was diluted in 35 mL of warm ethanol (200 proof), to which 20 mL of 4 μg/mL of HNO_3 solution in ethanol was added. The mixture was refluxed at 80 °C with stirring for 2 h. Then, a solution of 426.5 mg of iron(III) nitrate hydrate (99.999%, Alfa Aesar) and 68.7 mg of molybdenum(VI) oxide bis(2,4-pentanedionate) (99%, Alfa Aesar) in 20 mL of ethanol was added. The mixture was refluxed at 80 °C while stirring for 1 h and then cooled to room temperature. Gelation occurred after adding a solution containing 1 mL of ammonium hydroxide (trace metal grade, Fisher) and 1 mL of distilled water in 5 mL of ethanol, under intensive stirring. The gel was left to age overnight and supercritically dried at 270 °C and >100 atm the following day. The aerogel powder was calcinated in air flow at 500 °C for 1 h and heat-treated in argon flow at 820 °C for 1 h.

Alumina aerogel supported Pd catalyst (molar ratio Pd/Al_2O_3 = 1:17.5) was prepared in a similar way using 140 mg of palladium(II) nitrate (99.999%, Aldrich) and 5.26 g of aluminum *sec*-butoxide.

DSC Measurements. DSC measurements were performed on a STA 449C (NETZSCH) instrument that combines also TGA mea-

surement. The crucibles were alumina cups. In a typical experiment, ~5 mg of sample was heated at 5 °C/min in the temperature range of 20−1100 °C under Ar gas (150 sccm), diluted H_2 (20 sccm), and CH_4 or C_2H_4 flow (5 sccm). All the gases used had a purity of 99.999% (Praxair, Inc.), while $^{13}CH_4$ had a purity of 99.9% (Cambridge Isotope Laboratories, Inc.). All gases were passed through traps for H_2O and O_2 (VICI Mat/Sen) prior to feeding into the reactor.

Before introducing the gases, the system was evacuated for 4 h. The CH_4 gas was introduced after 60−80 min, when the system had stabilized for the given temperature.

MS Measurements. MS measurements on the gases exhausting the DSC apparatus were performed on a ThermoStar mass spectrometer (PFEIFFER Vacuum) attached to the gas outlet of the DSC apparatus.

GC Measurements. GC measurements were performed on Shimadzu GC17A with FID and methanizer by sampling the exhaust gas from the reactor in 2 L bags.

Raman Measurements. Raman spectra were collected in a ThermoNicolet spectrometer with CCD detector and laser excitations of 532 and 785 nm.

Acknowledgment. We thank B.I. Yakobson (Rice University) and K. Bolton (Göteborg University, Sweden) for valuable discussions and comments.

Supporting Information Available: Calorimetric curve for pure alumina powder and experimental details on the calorimetric measurements. This material is available free of charge *via* the Internet at http://pubs.acs.org.

REFERENCES AND NOTES

1. Baker, R. T. K.; Barber, M. A.; Waite, R. J.; Harris, P. S.; Feates, F. S. Nucleation and Growth of Carbon Deposits from the Nickel Catalyzed Decomposition of Acetylene. *J. Catal.* **1972**, *26*, 51–62.
2. Evans, E. L.; Thomas, J. M.; Thrower, P. A.; Walker, P. L. Growth of Filamentary Carbon on Metallic Surfaces during the Pyrolysis of Methane and Acetone. *Carbon* **1973**, *11*, 441–442.
3. Teo, K. B. K.; Singh, C.; Chhowalla, M.; Milne, W. I. *Encyclopedia of Nanoscience and Nanotechnology*; Nalwa, H. S., Ed.; American Scientific Publishers: California, 2003; Vol. 10, pp 1−22.
4. Helveg, S.; López-Cartes, C.; Sehested, J.; Hansen, P. L.; Clausen, B. S.; Rostrup-Nielsen, J. R.; Abild-Pedersen, F.; Nørskov, J. K. Atomic-Scale Imaging of Carbon Nanofibre Growth. *Nature* **2004**, *427*, 426–429.
5. Ajayan, P. M. How Does a Nanofibre Grow? *Nature* **2004**, *427*, 402–403.
6. Kanzow, H.; Ding, A. Formation Mechanism of Single-Wall Carbon Nanotubes on Liquid-Metal Particles. *Phys. Rev. B* **1999**, *60*, 11180–11186.
7. Harutyunyan, A. R.; Tokune, T.; Mora, E. Liquid as a Required Catalyst Phase for Carbon Single-Walled Nanotube Growth. *Appl. Phys. Lett.* **2005**, *87*, 051919-1–051919-3.
8. Cantoro, M.; Hofmann, S.; Pisana, S.; Scardaci, V.; Parvez, A.; Ducati, C.; Ferrari, A. C.; Blackburn, A. M.; Wang, K.-Y.; Robertson, J. Catalytic Chemical Vapor Deposition of Single-Wall Carbon Nanotubes at Low Temperatures. *Nano Lett.* **2006**, *6*, 1107–1112.
9. Diamond, S.; Wert, C. Diffusion of Carbon in Nickel above and below Curie Temperature. *Trans. Metall. Soc. AIME* **1967**, *239*, 705–709.
10. Rostrup-Nielsen, J. R.; Trimm, D. L. Mechanism of Carbon Formation on Nickel-Containing Catalysts. *J. Catal.* **1977**, *48*, 155–165.
11. Robertson, S. D. Carbon Formation from Methane Pyrolysis over Some Transition Metal Surfaces. II. Manner of Carbon and Graphite Formation. *Carbon* **1972**, *10*, 221–229.
12. Yang, R. T.; Chen, J. P. Mechanism of Carbon Filament Growth on Metal Catalysts. *J. Catal.* **1989**, *115*, 52–64.
13. Rostrup-Nielsen, J. R. Equilibria of Decomposition Reactions of Carbon Monoxide and Methane over Nickel Catalysts. *J. Catal.* **1972**, *27*, 343–356.
14. Cahill, D. G.; Ford, W. K.; Goodson, K. E.; Mahan, G. D.; Majumdar, A.; Maris, H. J.; Merlin, R.; Phillpot, S. R. Nanoscale Thermal Transport. *J. Appl. Phys.* **2003**, *93*, 793–818.
15. Eres, G; Kinkhabwala, A. A.; Cui, H.; Geohegan, D. B.; Puretzky, A. A.; Lowndes, D. H. Molecular Beam-Controlled Nucleation and Growth of Vertically Aligned Single-Wall Carbon Nanotube Arrays. *J. Phys. Chem. B* **2005**, *109*, 16684–16694.
16. Xu, Y. Q.; Flor, E.; Schmidt, H.; Smalley, R. E.; Hauge, R. H. Effects of Atomic Hydrogen and Active Carbon Species in 1 mm Vertically Aligned Single-Walled Carbon Nanotube Growth. *Appl. Phys. Lett.* **2006**, *89*, 123116.
17. Perdigon-Melon, J. A.; Auroux, A.; Bonnetot, B. Calorimetric Study of Methane Interaction with Supported Pd Catalysts. *J. Therm. Anal. Calorim.* **2003**, *72*, 443–451.
18. Klinke, C.; Bonard, J. M.; Kern, K. Thermodynamic Calculations on the Catalytic Growth of Multiwall Carbon Nanotubes. *Phys. Rev. B* **2005**, *71*, 035403.
19. Kurti, J.; Kresse, G.; Kuzmany, H. First-Principles Calculations of the Radial Breathing Mode of Single-Walled Carbon Nanotubes. *Phys. Rev. B* **1998**, *58*, R8869–R8872.
20. Reich, S.; Li, L.; Robertson, J. Structure and Formation Energy of Carbon Nanotube Caps. *Phys. Rev. B* **2005**, *72*, 165423.
21. Han, J. H.; Graff, R. A.; Welch, B.; Marsh, C. P.; Franks, R.; Strano, M. S. A Mechanochemical Model of Growth Termination in Vertical Carbon Nanotube Forests. *ACS Nano* **2008**, *2*, 53–60.
22. Crouse, C. A.; Maruyama, B.; Colorado, R., Jr.; Back, T.; Barron, A. R. Growth, New Growth, and Amplification of Carbon Nanotubes as a Function of Catalyst Composition. *J. Am. Chem. Soc.* **2008**, *130*, 7946–7954.
23. Qian, W.; Liu, T.; Wei, F.; Wang, Z.; Li, Y. Enhanced Production of Carbon Nanotubes: Combination of Catalyst Reduction and Methane Decomposition. *Appl. Catal., A* **2004**, *258*, 121–124.
24. Mora, E.; Pigos, J. M.; Ding, F.; Yakobson, B. I.; Harutyunyan, A. R. Low-Temperature Single-Wall Carbon Nanotubes Synthesis: Feedstock Decomposition Limited Growth. *J. Am. Chem. Soc.* **2008**, *130*, 11840–11841.
25. Hata, K.; Futaba, D. N.; Mizuno, K.; Namai, T.; Yumura, M.; Iijima, S. Water-Assisted Highly Efficient Synthesis of Impurity-Free Single-Walled Carbon Nanotubes. *Science* **2004**, *306*, 1362–1364.
26. Baker, R. T. K.; Harris, P. S. The Formation of Filamentous Carbon. In *Chemistry and Physics of Carbon*; Walker, P. L., Jr., Thrower, P. A., Eds.; Marcel Dekker: New York, 1978; Vol. 14, pp 83−165.
27. Ducati, C.; Alexandrou, I.; Chhowalla, M.; Amaratunga, G. A. J.; Robertson, J. Temperature Selective Growth of Carbon Nanotubes by Chemical Vapor Deposition. *J. Appl. Phys.* **2002**, *92*, 3299–3303.
28. Geohegan, D. B.; Puretzky, A. A.; Ivanov, I. N.; Jesse, S.; Eres, G.; Howe, J. Y. In Situ Growth Rate Measurements and Length Control during Chemical Vapor Deposition of Vertically Aligned Multiwall Carbon Nanotubes. *Appl. Phys. Lett.* **2003**, *83*, 1851–1853.
29. Li, Q.; Zhang, X.; DePaula, R. F.; Zheng, L.; Zhao, Y.; Stan, L.; Holesinger, T. G.; Arendt, P. N.; Peterson, D. E.; Zhu, Y. T. Sustained Growth of Ultralong Carbon Nanotube Arrays for Fiber Spinning. *Adv. Mater.* **2006**, *18*, 3160–3163.
30. Mora, E.; Harutyunyan, A. R. Study of Single-Walled Carbon Nanotubes Growth *via* the Catalyst Lifetime. *J. Phys. Chem. C* **2008**, *112*, 4805–4812.